Current Research in Food Science 10 (2025) 101039

Contents lists available at ScienceDirect

Current Research in Food Science

journal homepage: www.sciencedirect.com/journal/current-research-in-food-science

Bovine colostrum-derived extracellular vesicles protect against non-alcoholic steatohepatitis by modulating gut microbiota and enhancing gut barrier function

Daye Mun [a,1], Sangdon Ryu [b,1], Daniel Junpyo Lee [a], Min-Jin Kwak [a], Hyejin Choi [a], An Na Kang [a], Dong-Hyun Lim [c], Sangnam Oh [d,*], Younghoon Kim [a,**]

[a] Department of Agricultural Biotechnology and Research Institute of Agriculture and Life Science, Seoul National University, Seoul, 08826, Republic of Korea
[b] Honam National Institute of Biological Resources, Mokpo, 58762, Republic of Korea
[c] Dairy Science Division, National Institute of Animal Science, Rural Development Administration, Cheonan, 31000, South Korea
[d] Department of Functional Food and Biotechnology, Jeonju University, Jeonju, 55069, Republic of Korea

ARTICLE INFO

Handling Editor: Dr. Quancai Sun

Keywords:
Non-alcoholic steatohepatitis
Bovine colostrum-derived extracellular vesicles
Gut microbiota
Intestinal barrier function
Akkermansia
Gut–liver axis

ABSTRACT

Non-alcoholic steatohepatitis (NASH), characterized by severe fatty liver-associated inflammation and hepatocellular damage, is a major precursor to cirrhosis and hepatocellular carcinoma. While the exact pathogenesis of NASH remains unclear, gut microbiota dysbiosis has been implicated as a key factor contributing to endotoxin translocation and chronic liver inflammation. Recent studies have highlighted the therapeutic potential of bovine colostrum-derived extracellular vesicles (BCEVs) in modulating gut microbiota and enhancing gut barrier function, but their effects on NASH remain largely unexplored. To investigate the potential protective effects of BCEVs against NASH, 8-wk-old mice were fed a NASH-inducing diet for 3 wks while concurrently receiving oral BCEV administration. BCEV treatment markedly ameliorated hepatic steatosis, fibrosis, and inflammation. Transcriptomic analyses demonstrated a notable reduction in lipid metabolism, bacterial response, and inflammatory pathways in the intestine, as well as reduced expression of inflammation- and fibrosis-related pathways in the liver. Gut microbiota profiling revealed an increased abundance of *Akkermansia*, accompanied by enhanced cholesterol excretion. Furthermore, BCEV treatment promoted the production of tight junction proteins and mucin in the gut, reinforcing intestinal barrier integrity. These findings suggest that BCEVs promote the proliferation of *Akkermansia*, which in turn prevents endotoxin translocation to the liver. This reduction in endotoxin leakage alleviates hepatic inflammation and fibrosis. Overall, this study highlights the therapeutic potential of BCEVs as a novel strategy for managing NASH by targeting the gut–liver axis through the modulation of gut microbiota and barrier function.

1. Introduction

Non-alcoholic fatty liver disease (NAFLD) is among the leading causes of chronic liver disease, with its global prevalence rising markedly in recent years (Sheka et al., 2020). NAFLD encompasses a spectrum of liver conditions, ranging from simple hepatic steatosis (fat accumulation exceeding 5 %) to more severe stages such as steatohepatitis and cirrhosis, all of which are independent of alcohol consumption. Non-alcoholic steatohepatitis (NASH) is a more advanced form of NAFLD, characterized by hepatocellular damage, inflammation, and fibrosis (Brown and Kleiner, 2016). Approximately 25 % of adults with NASH progress to cirrhosis, and the disease is a well-established risk factor for liver cancer (Bugianesi et al., 2002). Despite its significant clinical impact, the pathogenesis of NASH remains complex and incompletely understood, and there are currently no approved therapies for its prevention or treatment. Therefore, ongoing research is focused on identifying bioactive compounds that may alleviate NASH and its associated complications.

Recent studies on the gut–liver axis have revealed a strong correlation between gut dysbiosis and chronic liver disease (Han et al., 2023).

* Corresponding author.
** Corresponding author.
E-mail addresses: osangnam@jj.ac.kr (S. Oh), ykeys2584@snu.ac.kr (Y. Kim).
[1] These authors contributed equally to the manuscript.

https://doi.org/10.1016/j.crfs.2025.101039
Received 23 January 2025; Received in revised form 5 March 2025; Accepted 22 March 2025
Available online 25 March 2025

Table 1
Primers used in this study for qRT-PCR.

Primer	Sequence (5'-3')
Krt18	Forward: CAAGTACTGGTCTCAGCAGATTGA
	Reverse: CTTGGTGGTGACAACTGTGGTA
Tgfb	Forward: GTCACTGGAGTTGTACGGCA
	Reverse: GGGCTGATCCCGTTGATTTC
Sma	Forward: GTCACTGGAGTTGTACGGCA
	Reverse: GGGCTGATCCCGTTGATTTC
Tnfa	Forward: GGTGCCTATGTCTCAGCCTCTT
	Reverse: GCCATAGAACTGATGAGAGGGAG
Il6	Forward: TACCACTTCACAAGTCGGAGGC
	Reverse: CTGCAAGTGCATCATCGTTGTTC
Muc2	Forward: ATGCCCACCTCCTCAAAGAC
	Reverse: GTAGTTTCCGTTGGAACAGTGAA
Cldn1	Forward: CGGGCAGATACAGTGCAAAG
	Reverse: ACTTCATGCCAATGGTGGAC
Ocln	Forward: ACCCGAAGAAAGATGGATCG
	Reverse: CATAGTCAGATGGGGGTGGA
Hprt1	Forward: TCAGTCAACGGGGGACATAAA
	Reverse: GGGGCTGTACTGCTTAACCAG

Gut dysbiosis increases intestinal permeability, allowing endotoxins such as lipopolysaccharides (LPS) to enter the bloodstream. These endotoxins are then transported to the liver, where they cause chronic inflammation (Liu et al., 2022). Prolonged exposure to endotoxins also promotes lipid accumulation in the liver, heightening the risk of progression to non-alcoholic steatohepatitis (Song and Zhang, 2022). Moreover, endotoxins that reach the liver interact with Toll-like receptor 4 (TLR4) on Kupffer cells, stimulating the production of inflammatory cytokines such as tumor necrosis factor-alpha (TNF-α) and interleukin-6 (IL-6), which contribute to hepatocyte damage and the development of NASH (Poeta et al., 2017). Therefore, restoring the balance of gut microbiota is considered a critical strategy for preventing NASH.

Extracellular vesicles (EVs) are biologically active vesicles secreted by most cell types. They contain nucleic acids, proteins, and lipids within their bilayer lipid membranes, playing a crucial role in intercellular communication (Gandham et al., 2020). Recent studies have highlighted the profound effects of EVs on various physiological and pathological processes, including immune responses and metabolic regulation (Wiklander et al., 2019).

Colostrum, secreted by mammals during the early stages of parturition, is widely recognized for its important immune and growth-promoting functions (Thapa, 2005). Our previous study demonstrated that bovine colostrum-derived EVs can ameliorate dextran sulfate sodium (DSS)-induced colitis by improving gut microbiota imbalance and upregulating inflammation-related miRNA genes (Mun et al., 2023). Moreover, milk-derived EVs have been reported to enhance host gut health and immune response. For instance, milk-derived exosomes improve the activity of antioxidant enzymes, such as superoxide dismutase (SOD) and glutathione peroxidase (GPC), under hydrogen peroxide (H_2O_2)-induced oxidative stress (Wang et al., 2021). Additionally, milk-derived EVs have been shown to influence lipid metabolism. Proteins and miRNAs present in human breast milk-derived EVs regulate lipid metabolism through the peroxisome proliferator-activated receptor (PPAR) and AMP-activated protein kinase (AMPK) signaling pathways, mitigating high-fat diet-induced fatty liver (Jiang et al., 2023). Furthermore, bovine mature milk-derived EVs have been shown to alleviate the symptoms of NASH by improving gut barrier function (Tong et al., 2023). However, to date, no studies have investigated whether colostrum-derived EVs can prevent NASH by modulating the gut microbiota. Therefore, this study was designed to investigate whether bovine colostrum-derived EVs (BCEVs) can modulate gut

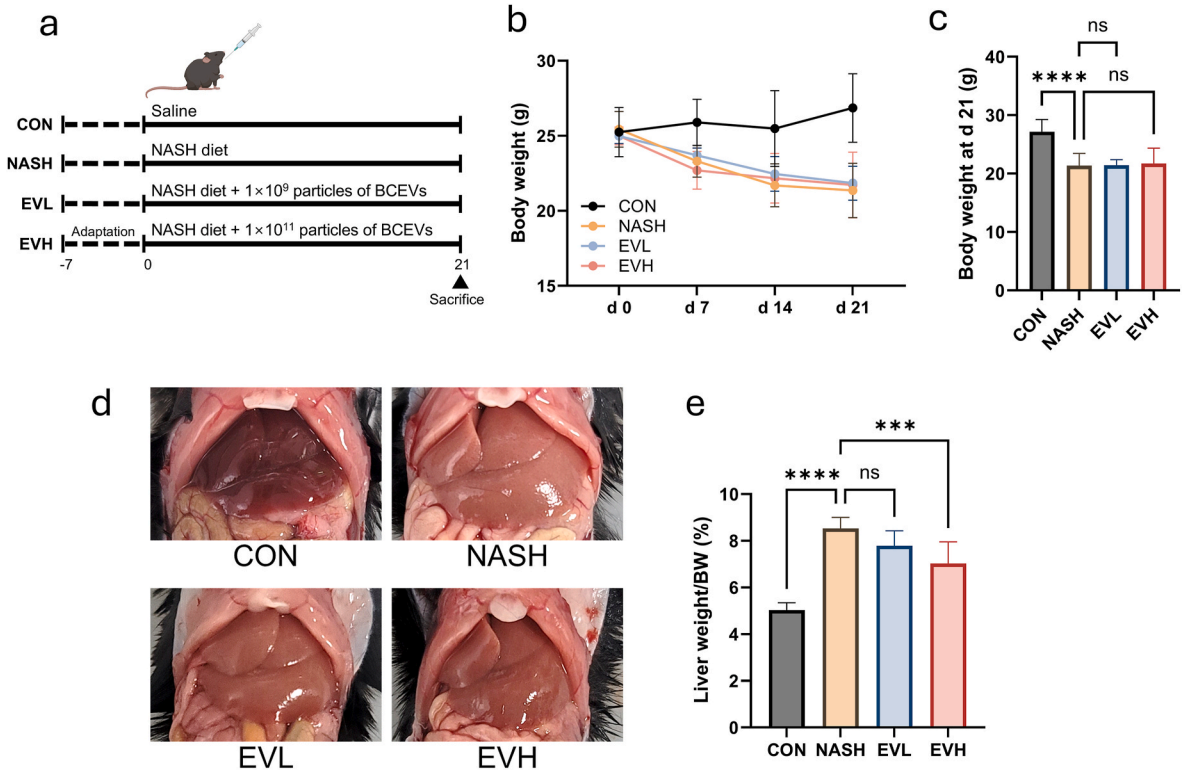

Fig. 1. Experimental design and physiological effects of BCEV treatment.
(a) Schematic of BCEV treatment via oral gavage (1×10^9 and 1×10^{11} particles/mouse for the EVL and EVH groups, respectively). b) Changes in body weight during BCEV treatment over 3 wks and (c) final body weight at day 21. (d) Representative liver image. (e) Liver weight. Data are presented as mean ± SD (n = 6). Differences among groups were analyzed using one-way ANOVA followed by Tukey's test. Asterisks indicate statistical significance: ***$p < 0.001$ and ****$p < 0.0001$. CON, saline control; NASH, NASH diet control; EVL, NASH diet with a low dose of BCEVs; EVH, NASH diet with a high dose of BCEVs.

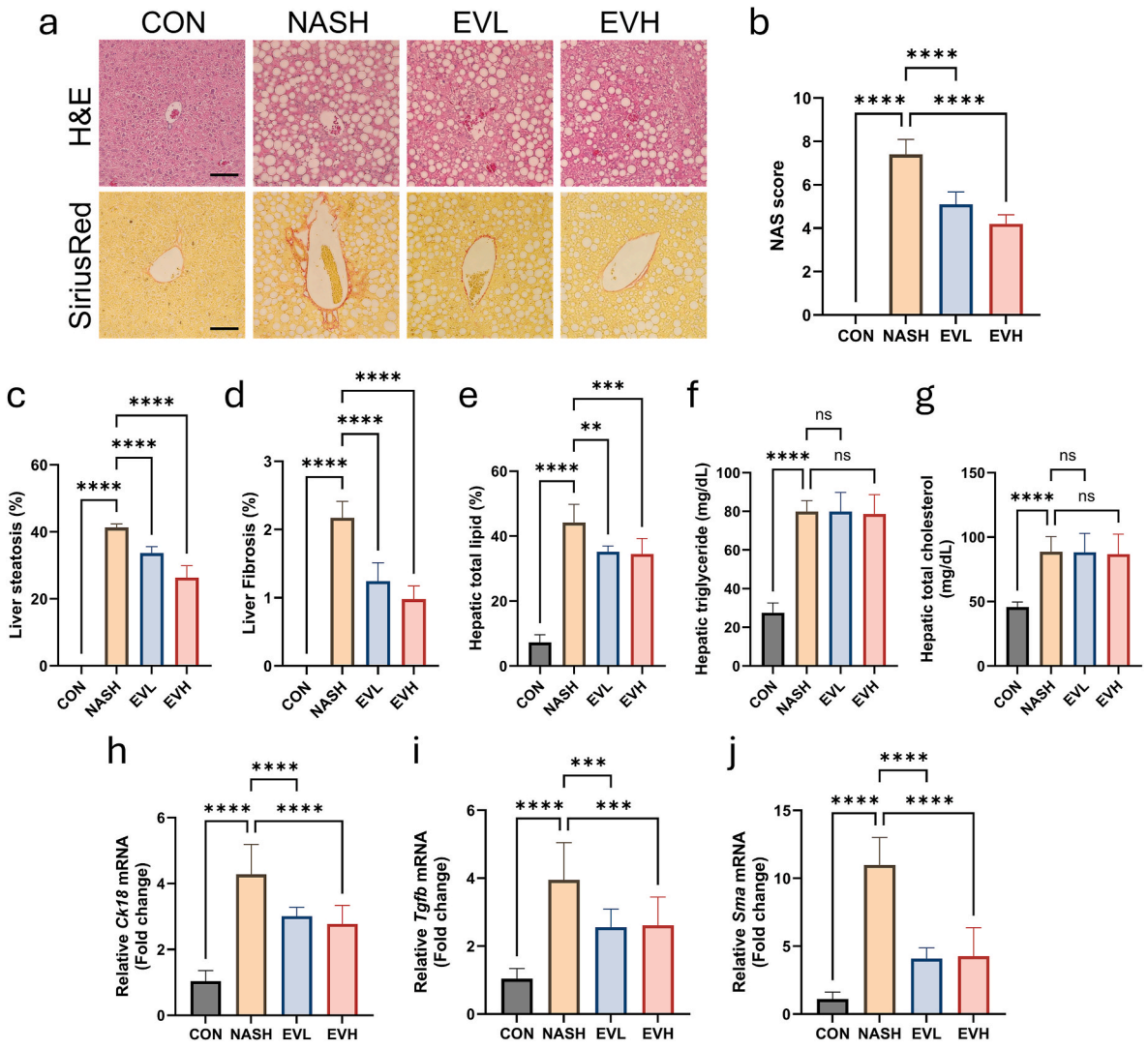

Fig. 2. Reduction in hepatic steatosis and fibrosis through BCEV treatment.
(a) Representative histological sections of the liver. Scale: 200 μm. b) Non-alcoholic Fatty Liver Disease Activity Score (NAS) of liver sections, along with (c) steatosis and (d) fibrosis areas. Hepatic (e) total lipid, (f) triglyceride, and (g) total cholesterol contents. (h–j) Hepatic mRNA expression levels of (h) NASH-related genes and fibrosis markers (i) *Tgfb* and (j) *Sma*. Data are presented as mean ± SD (n = 6). Differences among groups were analyzed using one-way ANOVA followed by Tukey's test. Asterisks indicate statistical significance: $^{**}p < 0.01$, $^{***}p < 0.001$, and $^{****}p < 0.0001$. CON, saline control; NASH, NASH diet control; EVL, NASH diet with a low dose of BCEVs; EVH, NASH diet with a high dose of BCEVs.

dysbiosis and offer protective effects against the resulting NASH.

2. Materials and methods

2.1. Isolation and characterization of EVs

Colostrum samples were collected within 3 d postpartum from healthy dairy cows at a conventional farm. To remove lipids, colostrum samples were initially centrifuged at 1200×*g* for 10 min, and cellular debris was subsequently removed by centrifugation at 16,000×*g* for 1 h. The whey fraction was obtained by further centrifugation of the supernatant at 100,000×*g* for 1 h. The obtained supernatant was further ultracentrifuged at 135,000×*g* for 90 min to pellet EVs. To ensure purity, the EV pellet was washed with phosphate-buffered saline (PBS) and centrifugation steps were repeated. The isolated EVs were resuspended in PBS and stored at −80 °C until further analysis. Ultracentrifugation was performed using a Beckman Coulter Optima XE-100 ultracentrifuge (Beckman Coulter, Brea, CA, USA). The average size and particle concentration of the isolated EVs were determined using nanoparticle tracking analysis (Malvern NanoSight NS300, Malvern Technologies, Malvern, UK).

2.2. Animals and treatment

All animal experiments were performed after review and approval by the Institutional Animal Care and Use Committee of Seoul National University (SNU-221101-2-2). Male C57BL/6 mice (7-wk-old) were purchased from OrientBio (Seongnam, South Korea) and housed under cotrolled conditions (12-h light/dark cycle, 55 ± 5 % humidity, 22 ± 1 °C). Mice were housed in individually ventilated cages with six mice per group ($n = 6$) and were allowed free access to water and food throughout the experimental period. Mice were randomized into four groups: CON (saline control), NASH (NASH-induced control), EVL (low concentration of BCEVs; 1×10^9 particles/mouse), and EVH (high concentration of BCEVs; 1×10^{11} particles/mouse). The higher dose was selected based on previous studies demonstrating its efficacy (Mun et al., 2023), while the lower dose was included to assess potential effects at a reduced concentration in the NASH model. NASH was induced by feeding mice a high-fat, fructose-supplemented, marginal methionine-supplemented, and choline-deficient diet for 3 wks, while

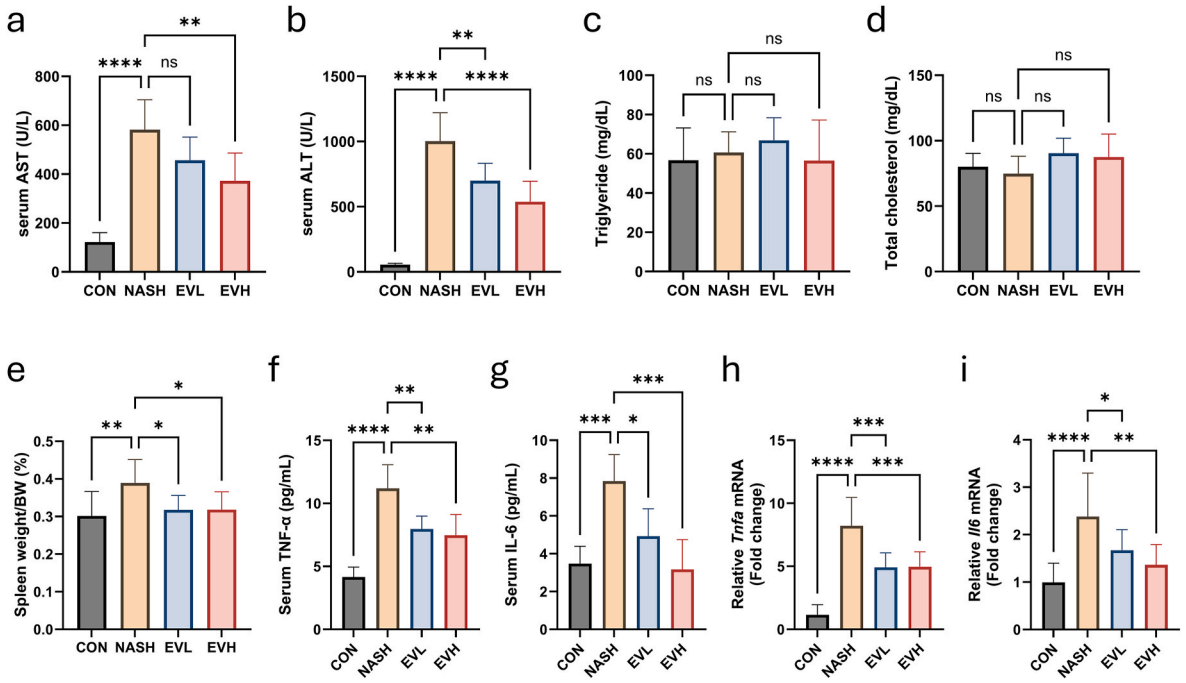

Fig. 3. Impact of BCEVs on serum biochemistry and inflammatory markers in NASH.
(a–d) Serum levels of (a) aspartate aminotransferase, (b) alanine aminotransferase, (c) triglycerides, and (d) total cholesterol. (e) Spleen weight. (f, g) Serum levels of the pro-inflammatory cytokines (f) TNF-α and (g) IL-6. (h, i) Hepatic mRNA expression levels of inflammatory markers (h) *Tnfa* and (i) *Il6*. Data are presented as mean ± SD (n = 6). Differences among groups were analyzed using one-way ANOVA followed by Tukey's test. Asterisks indicate statistical significance: $*p < 0.05$, $**p < 0.01$, $***p < 0.001$, and $****p < 0.0001$. CON, saline control; NASH, NASH diet control; EVL, NASH diet with a low dose of BCEVs; EVH, NASH diet with a high dose of BCEVs; AST, aspartate aminotransferase; ALT, alanine aminotransferase.

concurrently administering BCEVs orally.

2.3. Sample collection

The liver and spleen were weighed, and the liver-to-body weight ratio was calculated. Liver samples were fixed in 4 % paraformaldehyde solution and stored at 4 °C for tissue staining or frozen at −80 °C for RNA extraction. Colon, blood, and feces were collected for further analysis. For RNA extraction, colon tissue was washed with PBS to remove intestinal contents and frozen at −80 °C until use.

2.4. Liver staining and NAS scoring

Fixed liver tissue was stained with hematoxylin and eosin and Sirius Red to measure the Non-Alcoholic Fatty Liver Disease Activity Score (NAS) (Brunt et al., 2011). Briefly, NAS is determined by evaluating three histological factors: steatosis, lobular inflammation, and hepatocyte ballooning. Steatosis and lobular inflammation are each graded on a scale of 0–3, while hepatocyte ballooning is graded from 0 to 2, resulting in a total NAS ranging from 0 to 8. A score of 5 or higher is indicative of definite NASH, whereas a score of 3 or lower is classified as not NASH.

Total lipid in the liver was measured using the Folch method (Iverson et al., 2001). 100 mg of homogenized liver tissue was mixed with 2 mL of a hexane:isopropanol (3:2, v/v) solution and incubated under continuous rotation at 20 °C for 24 h. After incubation, 1 mL of sodium sulfate solution was added, followed by vortexing and centrifugation at 400×*g* for 10 min. The supernatant was collected in a new vial, and an additional 1 mL of hexane was added to the remaining liver sample to ensure complete lipid extraction. The mixture was rotated for another 24 h, vortexed, and centrifuged under the same conditions. The resulting supernatant was pooled with the previously collected fraction. The collected supernatant is vacuum-centrifuged for 2 h at 100 g to volatilize hexane, and the total lipid amount is calculated by measuring the weight of the remaining lipid. Triglyceride and total cholesterol levels were quantified using commercial kits (Embiel, Seoul, Korea), following the manufacturer's instructions. Three mL of the enzyme solution was mixed with 0.02 mL of the sample or standard solution and incubated at 37 °C for 5 min. Then, the concentration was determined by measuring the absorbance at 550 nm for triglycerides and 500 nm for total cholesterol.

2.5. Serum analysis

Mice blood samples were collected on the final day of the experiment and were allowed to clot at room temperature. The samples were then centrifuged at 3000×*g* for 15 min at 4 °C to obtain serum, which was stored at −80 °C until analysis. Aspartate transaminase (AST), alanine transaminase (ALT), triglyceride, and total cholesterol levels were measured using the Fuji DRI-CHEM Clinical Chemistry Analyzer FDC 3500 (Fujifilm, Tokyo, Japan). Serum samples were thawed on ice and centrifuged at 3000×*g* for 10 min at 4 °C to remove any residual debris. Each sample was then loaded into the analyzer, which automatically pipetted 10 μL of serum onto a Fuji DRI-CHEM slide specific to the target parameter. The slides were inserted into the analyzer, and the system processed the samples under standard conditions. Serum cytokines were analyzed using Mouse TNF-alpha and IL-6 ELISA Kits (R&D Systems, Inc., Minneapolis, MN), following the manufacturer's protocol. Briefly, 50 μL of serum samples, standards, and assay diluent were added to a 96-well plate and incubated at room temperature for 2 h. After washing, conjugate solution was added and incubated for another 2 h, followed by additional washing step. Substrate solution was then added and incubated in the dark for 30 min. Finally, stop solution was added, and absorbance was measured at 450 nm with a correction set to 540 or 570 nm. Cytokine concentrations were calculated from standard curves.

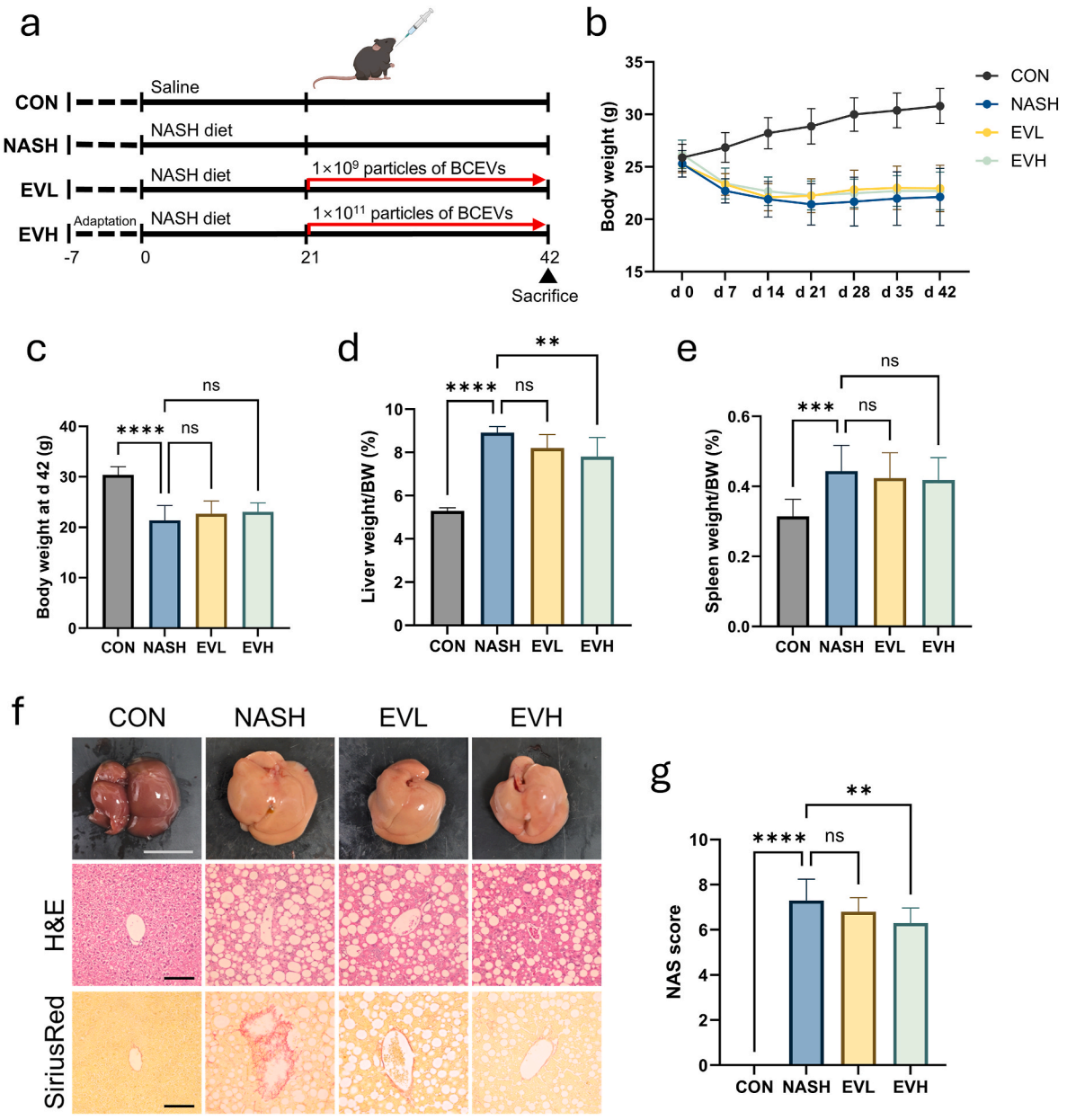

Fig. 4. Evaluating the therapeutic potential of BCEVs against NASH.
(a) Schematic representation of the experimental design. (b) Changes in body weight during BCEV treatment over 6 wks and (c) final body weight on day 42. (d) Liver weight. (e) Spleen weight. (f) Representative liver image (scale: 1 cm) and histological staining image (scale: 200 μm). (g) Non-alcoholic Fatty Liver Disease Activity Score (NAS). Data are presented as mean ± SD (n = 6). Differences among groups were analyzed using one-way ANOVA followed by Tukey's test. Asterisks indicate statistical significance: $^{**}p < 0.01$, $^{***}p < 0.001$, and $^{****}p < 0.0001$. CON, saline control; NASH, NASH diet control; EVL, NASH diet with a low dose of BCEVs; EVH, NASH diet with a high dose of BCEVs.

2.6. RNA isolation and quantitative real-time PCR (qRT-PCR) analysis

Total RNA was extracted using TRIzol reagent (Invitrogen, USA), and the RNeasy Plus Kit (Qiagen, Hilden, Germany), following the manufacturer's instructions. Tissue samples were homogenized in TRIzol, and chloroform was added for phase separation. The aqueous phase was collected and further purified using the RNeasy Plus Kit. Ethanol was added to the lysate before loading onto the spin column to enhance RNA binding. After several wash steps, RNA was eluted in nuclease-free water. RNA concentration and quality were assessed by measuring the 260/280 and 260/230 ratios using a spectrophotometer (SpectraMax ABS Plus, Molecular Devices, San Jose, CA). cDNA synthesis was performed using the iScript cDNA Synthesis Kit (Bio-rad, CA, USA). cDNA was synthesized from 1 μg of total RNA in a 20 μL reaction containing iScript Reaction Mix and iScript Reverse Transcriptase, followed by incubation in a thermal cycler at 25 °C for 5 min, 46 °C for 20 min, and 95 °C for 1 min qRT-PCR was conducted using the CFX96 System (Bio-rad, CA, USA) and the SsoAdvanced Universal SYBR Green Supermix. Each reaction was prepared in a 20 μL volume, including SYBR Green Supermix, gene-specific primers, and cDNA. The primer sequences used for qRT-PCR are listed in Table 1.

2.7. Transcriptomic analysis

RNA-sequencing (RNA-seq) was conducted using the TruSeq Stranded Total RNA Library Prep Gold Kit (Illumina, San Diego, CA, USA), following the manufacturer's protocol. Libraries were sequenced on an Illumina HiSeq 2000 platform with paired-end read sequencing (2

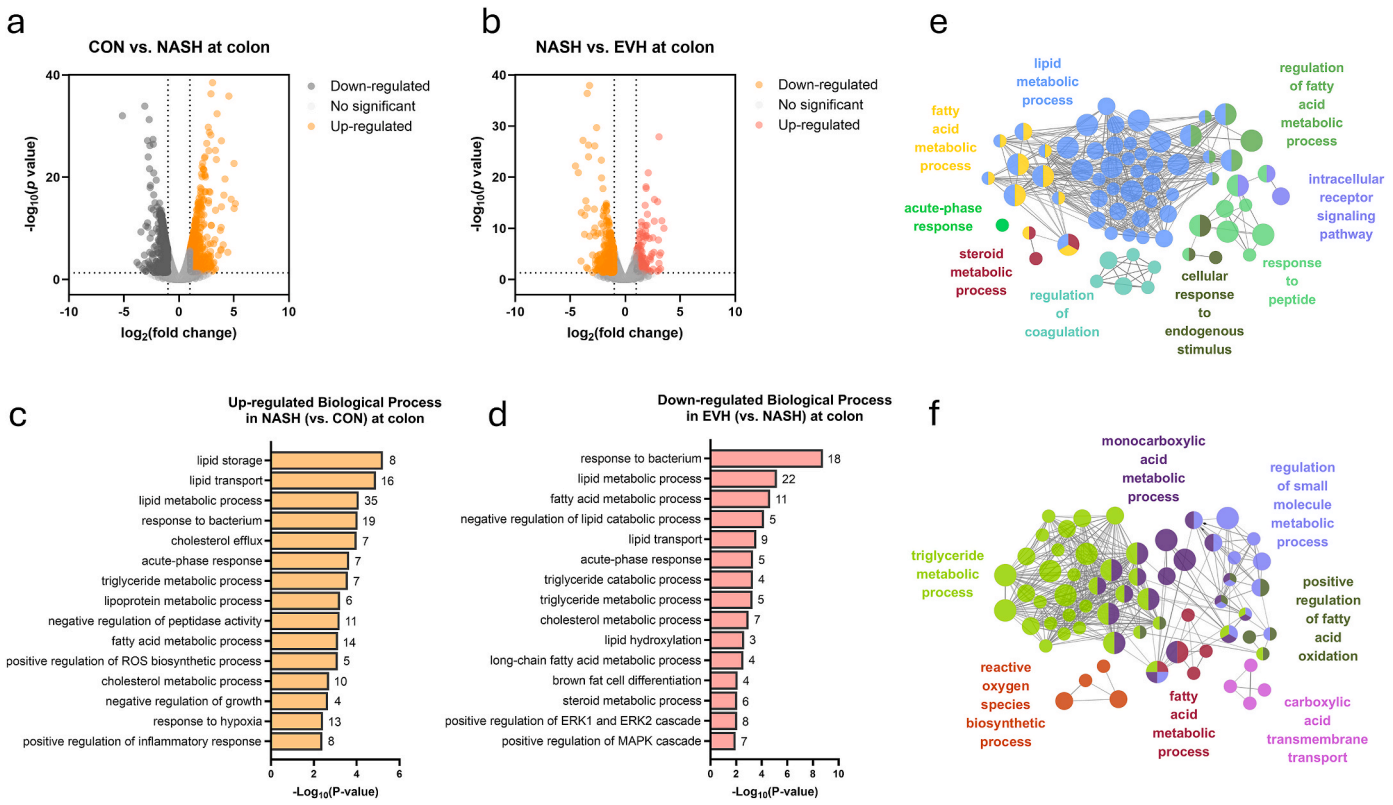

Fig. 5. Impact of BCEVs on gene expression and functional networks in the colon.
(a, b) Volcano plots of differentially expressed genes (DEGs) in the colon: (a) between CON and NASH and (b) between NASH and EVH groups. Colored dots indicate DEGs selected with cutoff criteria of $p < 0.05$ and absolute [log 2 (fold change)] > 1. (c, d) Gene Ontology (GO) analysis of RNA-seq results: (c) between CON and NASH groups and (d) between NASH and EVH groups. (e, f) Enriched GO network visualization using the ClueGO plugin of Cytoscape, showing functionally grouped networks for DEGs associated with immune system processes and biological processes: (e) between CON and NASH groups and (f) between NASH and EVH groups. CON, saline control; NASH, NASH diet control; EVH, NASH diet with a high dose of BCEVs.

× 150 bp). Raw reads were processed using Trimmomatic 0.38 (Bolger et al., 2014) to remove adapter sequences. Preprocessed reads were mapped to a reference genome using the HISAT2 program (Kim et al., 2015). Subsequently, transcript assembly was performed using the StringTie program (Pertea et al., 2015), yielding expression profile values for each sample. Metrics such as read count, Fragment per Kilobase of transcript per Million mapped reads (FPKM), and Transcripts Per Kilobase Million (TPM) were calculated and organized based on transcript/gene. Differentially expressed genes (DEGs) were analyzed using edgeR (Robinson et al., 2010) by extracting genes that satisfied the criteria of $|fc| \geq 2$ and a raw p-value <0.05 (calculated using the exactTest function) in at least one comparison. Gene set enrichment analysis for significant DEGs was performed using gProfiler and DAVID to classify genes by biological process (BP), molecular function (MF), and cellular component (CC), as defined by gene ontology (Jr et al., 2003). The sequence data generated in this study were deposited in the Gene Expression Omnibus database under the project accession number GSE273582 (https://www.ncbi.nlm.nih.gov/geo).

2.8. Metabolomic analysis

Each fecal sample was diluted in methanol to a final concentration of 40 mg/mL and vortexed on ice for 5 min. The samples were then centrifuged at 15,000×g for 5 min at 4 °C, and the supernatant was filtered through 0.2 μm pore size polyvinylidene fluoride (PVDF) syringe filters (Whatman, Maidstone, England). A 200 μL aliquot of the filtered supernatant was dried in a vacuum concentrator and derivatized by adding 30 μL of a 20 mg/mL methoxyamine hydrochloride solution in pyridine (Sigma, St. Louis, USA), followed by incubation at 30 °C for 90 min. Subsequently, 50 μL of N,O-bis(trimethylsilyl)trifluoroacetamide (BSTFA; Sigma, St. Louis, USA) was added, and the sample was incubated at 60 °C for 30 min. GC-MS analysis was performed using a Thermo Trace 1310 GC (Waltham, MA, USA) system coupled to a Thermo ISQ LT single quadrupole mass spectrometer (Waltham, MA, USA), following a previously described protocol (Yoo et al., 2022). Metabolites were identified by matching mass spectra with the NIST Mass Spectral Search Program (version 2.0, Gaithersburg, MD, USA). Further statistical analysis was performed using MetaboAnalyst 5.0 (Pang et al., 2021). Data were auto-scaled before multivariate statistical analyses. Partial least squares-discriminant analysis (PLS-DA) was performed to assess group separation and identify discriminative metabolites. Variable importance in projection (VIP) scores were calculated to rank the most influential metabolites contributing to group differentiation. Heatmap analysis was conducted to visualize metabolite abundance patterns across experimental groups.

2.9. Microbiome analysis using 16S rRNA amplicon sequencing

Fecal DNA was extracted using the PowerFecal DNA Isolation Kit (Qiagen, Hilden, Germany). The V3–V4 region of the 16S rRNA gene was amplified using PCR and sequenced on a Nextseq platform (2 × 300 bp) (Illumina Inc., San Diego, CA, USA) at Sanigen Inc., Korea, following the manufacturer's instructions. Sequenced raw data was subjected to demultiplexing and quality control (QC), followed by adapter trimming, quality trimming, error correction of reads, and removal of chimeric sequences. Amplicon sequence variants (ASVs) were generated using the Divisive Amplicon Denoising Algorithm 2 (DADA2) via the QIIME 2 plugin. For taxonomy analysis, classification was performed using the SILVA 138.1 database (Quast et al., 2012), mitochondrial and chloroplast sequences were removed, alignment was performed, and alpha and

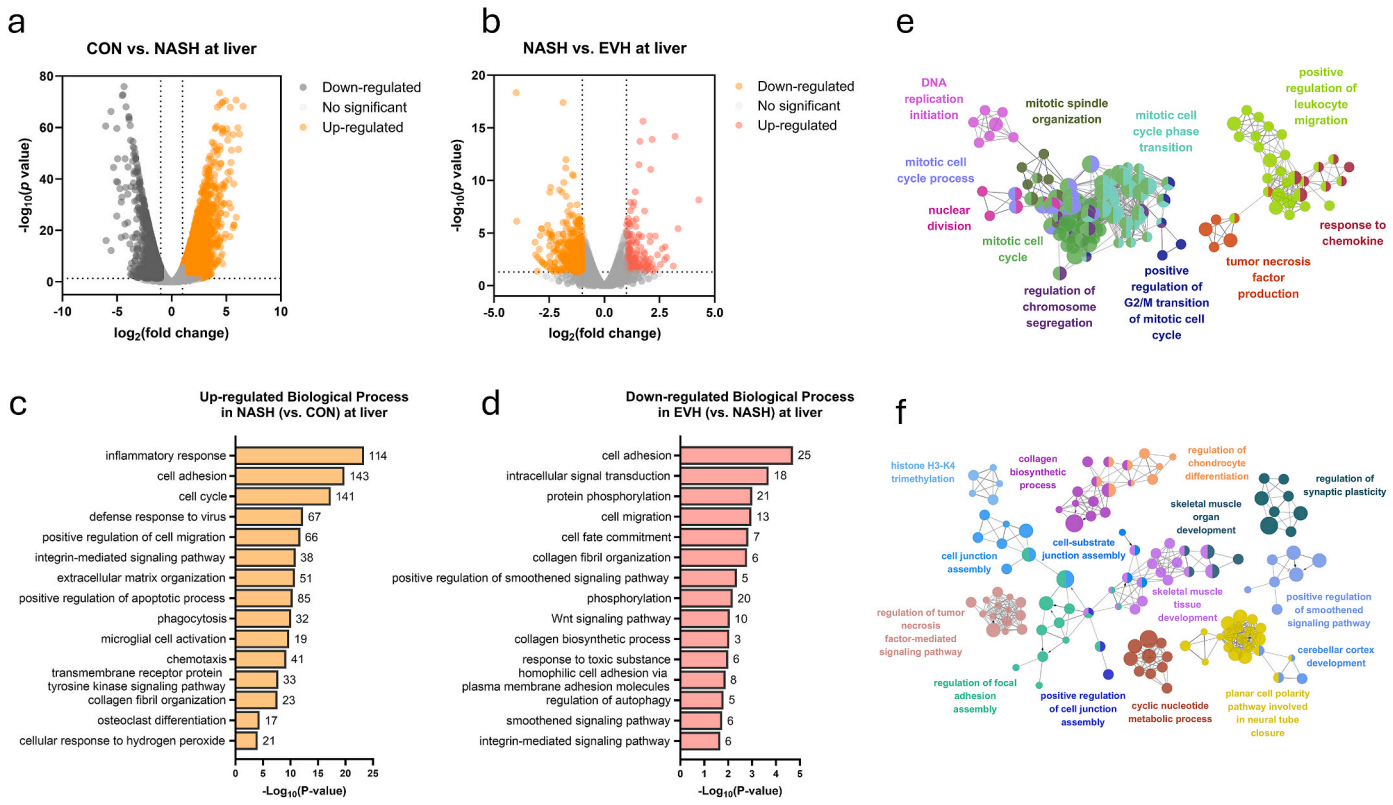

Fig. 6. Impact of BCEVs on gene expression and functional networks in the liver.
(a, b) Volcano plots of differentially expressed genes (DEGs) in the liver: (a) between CON and NASH and (b) between NASH and EVH groups. Colored dots indicate DEGs selected with cutoff criteria of $p < 0.05$ and absolute [log 2 (fold change)] > 1. (c, d) Gene Ontology (GO) analysis of RNA-seq results: (c) between CON and NASH groups and (d) between NASH and EVH groups. (e, f) Enriched GO network visualization using the ClueGO plugin of Cytoscape, showing functionally grouped networks for DEGs associated with immune system processes and biological processes: (e) between CON and NASH groups and (f) between NASH and EVH groups. CON, saline control; NASH, NASH diet control; EVH, NASH diet with a high dose of BCEVs.

beta diversity were analyzed. Principal component analysis (PCA) and Welch's *t*-test were performed using Statistical Analysis of Taxonomic and Functional Profiles (STAMP) software (Parks et al., 2014). PCA was applied to visualize sample clustering based on microbial composition. Welch's *t*-test was conducted to identify significantly different taxa between groups. Effect sizes and confidence intervals were calculated to assess the biological relevance of significant features, and results were visualized using bar plots and extended error bar plots. The correlations between gut microbiota and metabolites were analyzed using Pearson correlation analysis in R software. The sequence data generated in this study were deposited in the Short Read Archives under the project accession number PRJNA1133920 (https://www.ncbi.nlm.nih.gov/sra).

2.10. Statistical analysis

Statistical analyses were performed using GraphPad Prism 10.0 software (GraphPad Software, San Diego, CA, USA). Differences between groups were assessed using the Student's *t*-test, and multiple group comparisons were performed using one-way analysis of variance (ANOVA) followed by Tukey's post hoc test. Results were considered statistically significant at $p < 0.05$. Data are expressed as mean ± standard deviation (SD).

3. Results

3.1. BCEVs protect against NASH pathophysiology

To evaluate whether BCEVs mitigate NASH, a mouse model was established by feeding mice a high-fat, high-fructose diet deficient in choline and minimally supplemented with methionine for 3 wks (Fig. 1a). Concurrently, BCEVs were administered daily via oral gavage throughout the experimental period. Changes in body weight were monitored throughout the experiment, and the results showed significant weight loss in the three groups fed the NASH diet compared to the CON group (Fig. 1b and c). The NASH group exhibited enlarged, pale livers, a condition that was partially ameliorated in the high-concentration BCEV group (i.e., the EVH group) (Fig. 1d). Additionally, the increase in liver weight associated with NASH was significantly reduced in the EVH group (Fig. 1e).

3.2. BCEVs ameliorate NASH by reducing hepatic steatosis and fibrosis

To assess whether BCEVs alleviate hepatic lipid accumulation and fibrosis, histological analysis of the liver was performed. H&E staining revealed a significant increase in lipid droplets in the NASH group, along with marked hepatocyte ballooning and inflammatory cell infiltration (Fig. 2a). BCEV administration significantly reduced lipid accumulation and NAS scores at both doses (Fig. 2b and c). Sirius Red staining demonstrated a notable increase in fibrosis, consistent with severe steatosis in the NASH group. Conversely, a significant decrease in the fibrosis area was observed in the liver sections of both the EVL and EVH groups (Fig. 2d). To validate the reduction in hepatic lipid content, total lipids were extracted from liver samples (Fig. 2e). The results indicated that the significantly elevated hepatic lipid content in the NASH group was reduced following BCEV administration, aligning with histological findings. However, the triglyceride and total cholesterol levels in the liver did not differ among the NASH induction groups (Fig. 2f and g).

Furthermore, the expression of the *Ck18* gene, a well-known NASH biomarker, was significantly upregulated in the NASH group and

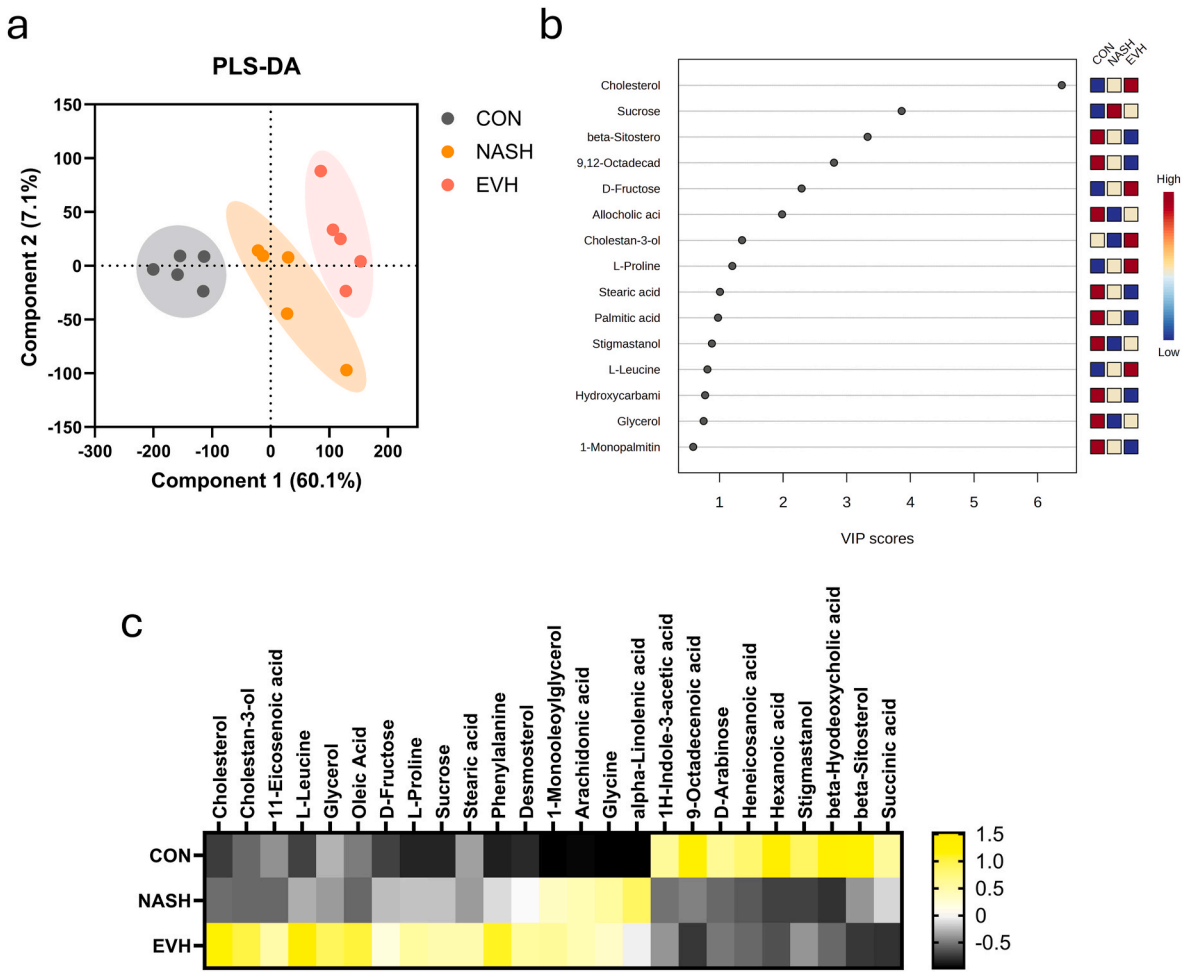

Fig. 7. Alterations in fecal metabolites associated with BCEV treatment
(a) PLS-DA analysis of metabolites. (b) VIP score of PLS-DA analysis. (c) Heat map showing changes in metabolites. CON, saline control; NASH, NASH diet control; EVH, NASH diet with a high dose of BCEVs; PLS-DA, partial least squares discriminant analysis; VIP, variable importance in projection.

significantly reduced in both the EVL and EVH groups (Fig. 2h). Additionally, the expression of the *Tgfb* and *Sma* genes, markers of fibrosis, increased significantly in the NASH induction groups, corroborating previous staining results (Fig. 2i and j), and decreased following BCEV administration. Collectively, these findings suggest that oral BCEVs can effectively prevent intrahepatic lipid accumulation and fibrosis.

3.3. BCEVs alleviate NASH by reducing hepatic toxicity and modulating inflammation

To assess the impact of BCEVs on systemic immune response and hepatotoxicity, a blood biochemical analysis was conducted. Serum levels of both AST and ALT were significantly elevated in the NASH group compared to the CON group, with AST and ALT levels increasing 4.7-fold and 18-fold, respectively (Fig. 3a and b). Notably, high-dose BCEV treatment significantly reduced AST levels (by 63 %; Fig. 3a). Additionally, ALT levels were significantly reduced in both the EVL and EVH groups, with reductions of 69 % and 76 %, respectively (Fig. 3b). No significant difference in serum triglyceride and total cholesterol levels was observed across all groups (Fig. 3c and d).

Spleen weight, a marker of immune response, was significantly elevated in the NASH group but notably reduced following BCEV treatment (Fig. 3e). Additionally, serum levels of inflammatory cytokines declined following BCEV treatment, indicating that BCEVs mitigate the NASH-induced elevations in inflammatory markers (Fig. 3f and g). Specifically, the expression of *Tnfa* and *Il6*, which were upregulated in the liver of NASH-induced mice, was downregulated in both the EVL and EVH groups (Fig. 3h and i). These findings suggest that pretreatment with BCEVs helps mitigate NASH-induced liver toxicity and the associated inflammatory response.

3.4. BCEVs ameliorate NASH symptoms through post-induction treatment

Based on the findings that BCEV treatment could prevent NASH symptoms, the potential of post-induction treatment to improve NASH was investigated. Mice were first fed a NASH-inducing diet for 3 wks to induce NASH, followed by an additional 3 wks on the same diet alongside daily oral administration of BCEVs, for a total duration of 6 wks (Fig. 4a). During the experiment, body weight changes did not differ significantly among the NASH diet groups (Fig. 4b and c). However, liver weight as a percentage of body weight was significantly reduced only in the high-dose BCEV group (i.e., the EVH group; Fig. 4d), while no significant differences in spleen weight were observed among the NASH diet groups (Fig. 4e). Representative liver images showed that BCEV treatment alleviated NASH-induced liver enlargement (Fig. 4f). Histological analysis revealed that high-dose BCEV treatment significantly improved steatosis and fibrosis, as indicated by a marked reduction in the NAS score (Fig. 4g). These results underscore the effectiveness of high doses of BCEVs in ameliorating NASH.

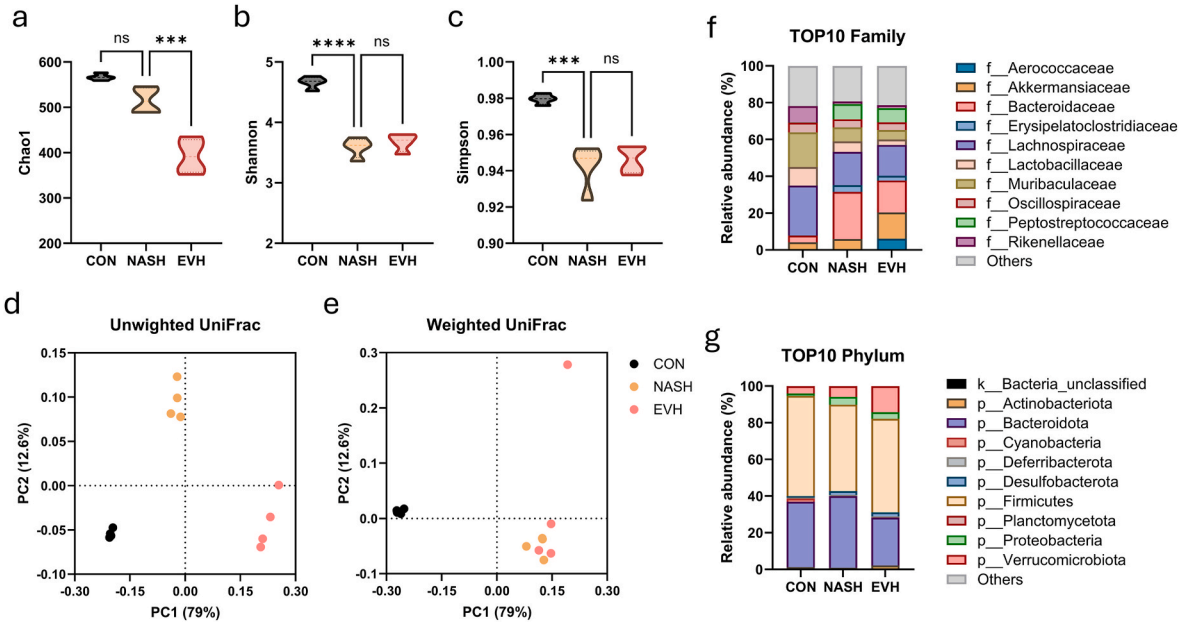

Fig. 8. Alterations in gut microbiota diversity and relative abundance following BCEV treatment
(a–c) Alpha diversity analysis using (a) Chao1 index, (b) Shannon index, and (c) Simpson index. (b, e) Beta diversity analysis using (d) Unweighted UniFrac and (e) Weighted UniFrac indices. (f, g) Related abundance (%) of the top 10 (f) phyla and (g) family of gut microbiota. Data are presented as mean ± SD (n = 4, randomly selected from 6). Differences among groups were analyzed using one-way ANOVA followed by Tukey's test. Asterisks indicate statistical significance: ***$p < 0.001$, and ****$p < 0.0001$. CON, saline control; NASH, NASH diet control; EVH, NASH diet with a high dose of BCEVs.

3.5. BCEVs suppress NASH-induced bacterial response and inflammation in the intestine

To explore the mechanisms through which BCEV treatment improves NASH in the gut–liver axis, transcriptomics analysis was performed. In the intestine, 730 genes were upregulated, and 454 genes were downregulated in the NASH group compared to the CON group (Fig. 5a). In contrast, in the BCEV-treated groups, 149 genes were upregulated, and 329 genes were downregulated compared to the NASH-induced group (Fig. 5b). Gene enrichment analysis, performed using DAVID, revealed that genes involved in lipid metabolism, bacterial response, reactive oxygen species production, and immune response were upregulated in the intestine of NASH-induced mice compared to the CON group (Fig. 5c). Conversely, genes related to bacterial response were significantly reduced in the BCEV-treated groups compared to the NASH group, along with a decrease in biological processes related to lipid metabolism, fatty acid metabolism, and the acute-phase response (Fig. 5d). Further analysis of the DEGs using the Cytoscape ClueGo platform revealed that genes associated with intestinal lipid metabolism and stress-related signaling pathways were closely linked to NASH (Fig. 5e). BCEV treatment significantly downregulated genes involved in triglyceride metabolism and reactive oxygen species production (Fig. 5f). These results confirm that NASH induces bacterial infection, inflammation, and disruption of the lipid metabolism in the intestine and that BCEV treatment effectively inhibits these processes.

3.6. BCEVs inhibit NASH-induced immune responses and fibrosis in the liver

To evaluate the impact of BCEVs on liver inflammation and fibrosis in NASH, changes in global transcriptome expression were analyzed across experimental groups. DEG analysis revealed that NASH induction resulted in 2614 significantly upregulated and 1550 downregulated genes in the liver compared to the CON group (Fig. 6a). BCEV treatment in NASH-induced mice led to 252 upregulated and 486 downregulated genes compared to the untreated NASH group (Fig. 6b). Gene enrichment analysis indicated that inflammatory response pathways were significantly elevated in the NASH liver, with upregulation observed in genes related to cell adhesion and cell cycle (Fig. 6c). Conversely, genes associated with cell adhesion, intracellular transduction, cell migration, and collagen biosynthesis— processes linked to liver fibrosis—were significantly downregulated in the BCEV-treated groups compared to the NASH group (Fig. 6d). Visualization of DEGs highlighted an upregulation of genes involved in the cell cycle and leukocyte regulation, forming distinct networks in the liver of NASH-induced mice (Fig. 6e). BCEV treatment effectively reduced the expression of genes related to collagen biosynthesis, cell junction assembly, and immune responses in the liver (Fig. 6f). These results confirm that BCEV treatment reduces the expression of inflammation and fibrosis-related genes elevated in NASH-induced liver.

3.7. BCEVs increase cholesterol excretion

To determine the effects of BCEVs on metabolic processes in the gut, fecal metabolomics analysis was performed. A total of 95 metabolites were identified, including amino acids, organic acids, lipids, fatty acids, and alcohols. PLS-DA revealed significant differences in the metabolome across the groups (Fig. 7a). VIP score highlighted cholesterol as the metabolite most distinctly differentiating the groups (Fig. 7b). Analysis of key metabolites showed that L-proline, phenylalanine, and glycine were significantly elevated in the NASH group compared to the CON group. Conversely, metabolites such as hexanoic acid, D-arabinose, and heneicosanoic acid were significantly lower in the NASH group. Compared to the NASH group, metabolites such as cholestan-3-ol, cholesterol, and 11-eicosenoic acid were significantly increased in the EVH group (Fig. 7c). These findings demonstrate that BCEV treatment decreases metabolites related to lipid metabolism while promoting fecal cholesterol excretion, indicating its potential role in mitigating NASH-related metabolic dysregulation.

3.8. BCEVs enhance the abundance of Akkermansia in the fecal microbiota of NASH-induced mice

To investigate the impact of BCEVs on the gut microbiota, fecal

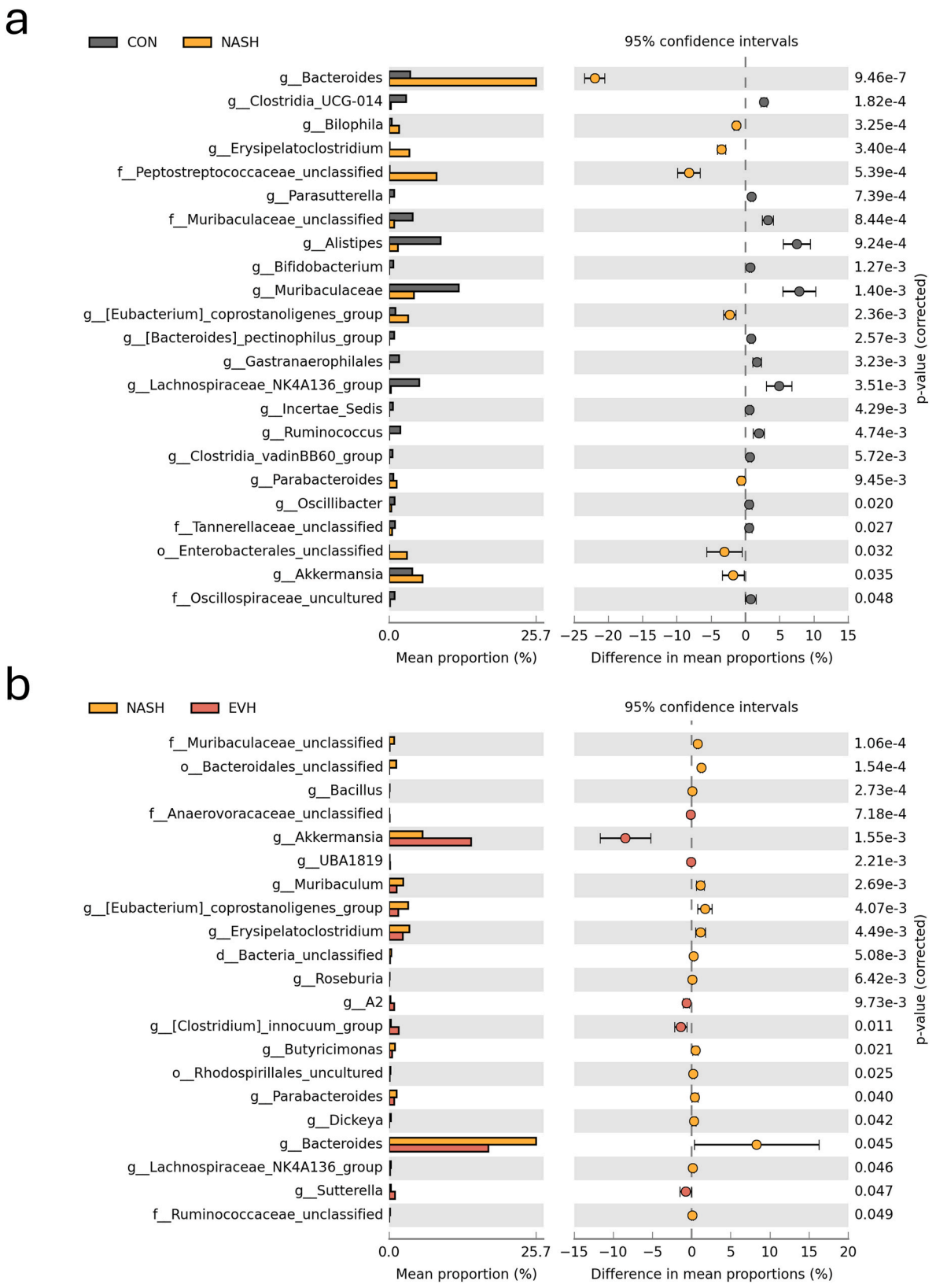

Fig. 9. Comparison of significantly different genera of gut microbiota.
(a, b) Analysis of differential abundance: (a) between CON and NASH samples and (b) between NASH and EVH samples. CON, saline control; NASH, NASH diet control; EVH, NASH diet with a high dose of BCEVs.

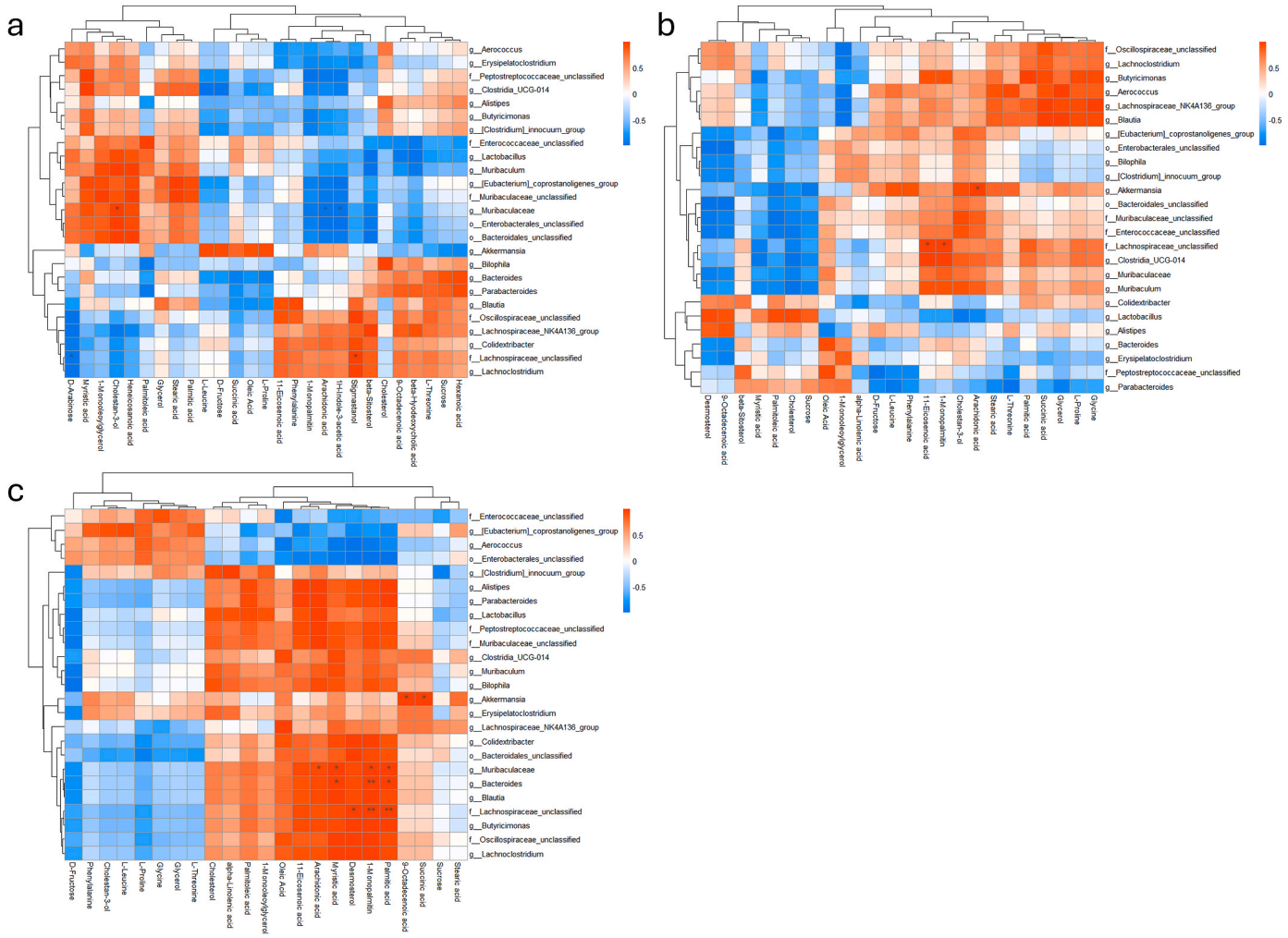

Fig. 10. Correlation analysis between gut microbiota and metabolites.
(a–c) The heatmap shows the correlation between gut microbiota and metabolites in the (a) CON, (b) NASH, and (c) EVH groups. Positive correlations are shown in red, and negative correlations are shown in blue, with darker colors indicating stronger correlations. Asterisks indicate statistical significance: $*p < 0.05$ and $**p < 0.01$. CON, saline control; NASH, NASH diet control; EVH, NASH diet with a high dose of BCEVs.

samples were collected from each group on the final day of the experiment and subjected to 16S metagenomic analysis. A total of 8,296,727 read pairs (ranging from 586,979 to 808,691 reads per sample) were generated and subjected to denoising and filtering. In total, 3288 features were identified across all samples. Alpha diversity analysis revealed no significant differences in the Chao 1 index between the CON and NASH groups, but the EVH group showed a significant decrease (Fig. 8a). The Shannon index and Simpson indices were both significantly lower in the NASH-induced groups compared to the CON group (Fig. 8b and c). PCA plot demonstrated distinct clustering of the three groups ($p < 0.05$) in both Unweighted UniFrac and Weighted UniFrac (Fig. 8d and e).

At the phylum level, a significant decrease in the abundance of Firmicutes and an increase in the abundance of Bacteroidota were observed in the NASH compared to the CON group (Fig. 8f). In the EVH group, the abundance of Verrucomicrobiota was significantly increased, while that of Bacteroidota was significantly decreased compared to the NASH group. At the family level, the abundance of *Bacteroidaceae*, *Erysipelatoclostridiaceae*, and *Peptostreptococcaceae* was significantly elevated in the NASH group compared to the CON group (Fig. 8g). Conversely, in the EVH group, the abundance of *Akkermansiaceae* was significantly increased and that of *Bacteroidaceae* was decreased compared to the NASH group.

At the genus level, the abundance of *Bacteroides* increased by approximately 25 % in the NASH group compared to the CON group, alongside significant increases in the abundance of *Bilophila* and *Erysipelatoclostridium*, and decreases in the abundance of *Alistipes*, *Bifidobacterium*, *Muribaculum*, and *Ruminococcus* (Fig. 9a). In the EVH group, the abundance of *Bacteroides*, *Muribaculum*, *Erysipelatoclostridium*, and *Parabacteroides* decreased, while that of *Sutterella* and *Akkermansia* increased significantly compared to the NASH group (Fig. 9b). These results suggest that oral administration of BCEVs modulates the intestinal microbiota, notably reducing the abundance of *Bacteroides* and significantly increasing the abundance of *Akkermansia*, which is associated with the alleviation of NASH symptoms.

3.9. BCEVs modulate the gut microbiota and correlated metabolites to improve NASH

To investigate the relationship between the gut microbiota and gut metabolites in each group, we analyzed the correlation between the top 25 genera and metabolites. In the CON group, Muribaculaceae-affiliated genera showed a negative correlation with 1H-indole-3-acetic acid and arachidonic acid, and a significant positive correlation with cholestan-3-ol. In addition, Lachnospiraceae_unclassified had a significant positive correlation with stigmastanol and a negative correlation with D-arabinose (Fig. 10a). In the NASH group, the *Akkermansia* demonstrated a significant positive correlation with arachidonic acid, whereas

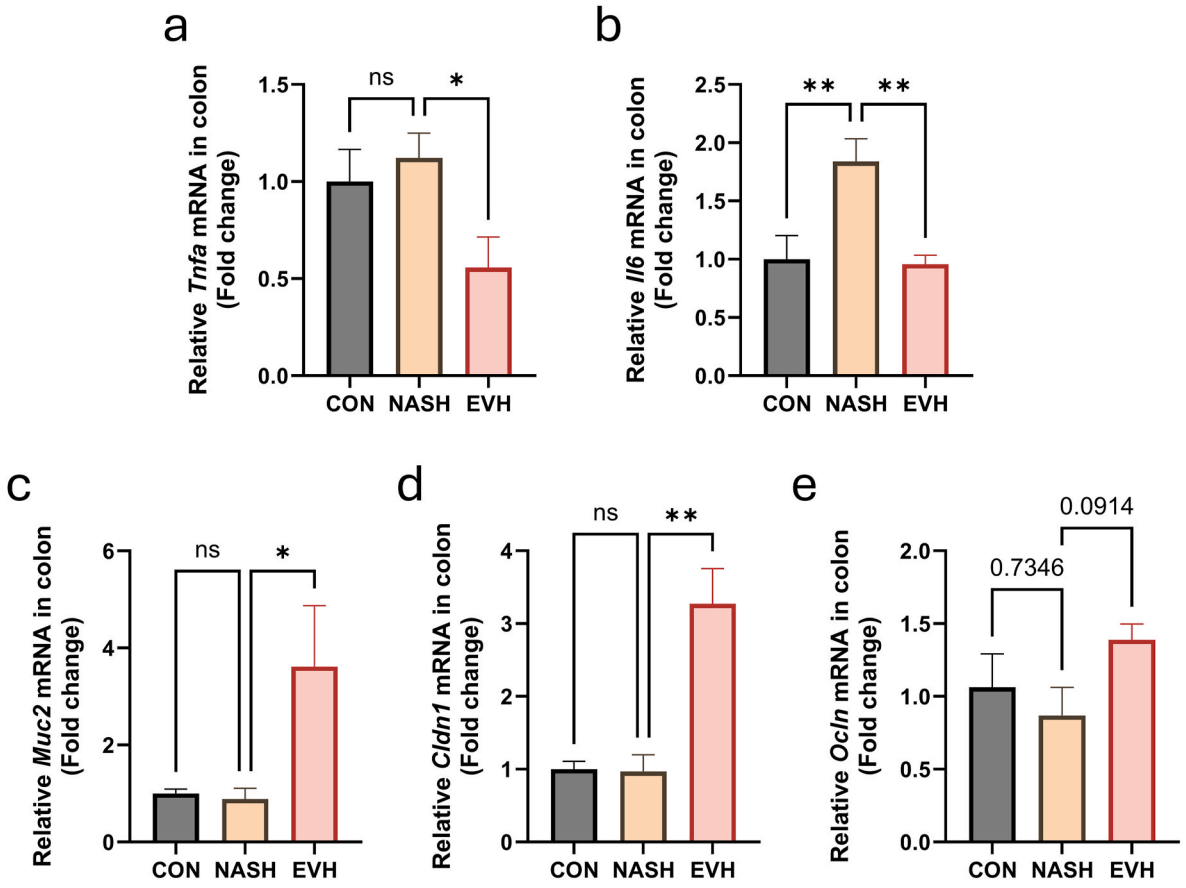

Fig. 11. Fold changes in mRNA expression related to inflammation and intestinal barrier function.
(a–e) The mRNA expression levels of (a) *Tnfa,* (b) *Il6,* (c) *Muc2*, (d) *Cldn1*, and (e) *Ocln* were analyzed using qRT-PCR. Data are presented as mean ± SD (n = 6). Differences among groups were analyzed using one-way ANOVA followed by Tukey's test. Asterisks indicate statistical significance: $*p < 0.05$ and $**p < 0.01$. CON, saline control; NASH, NASH diet control; EVH, NASH diet with a high dose of BCEVs.

Lachnospiraceae_unclassified exhibited significant positive correlations with 1-monopalmitin and 11-eicosenoic acid (Fig. 10b). In the EVH group, the *Akkermansia* was significantly positively correlated with succinic acid and 9-octadecenoic acid. Furthermore, Muribaculaceae-affiliated genera, *Bacteroides*, and Lachnospiraceae_unclassified exhibited significant positive correlations with palmitic acid, 1-monopalmitin, desmosterol, myristic acid, and arachidonic acid (Fig. 10c). Taken together, these results suggest that bacterial taxa belonging to the *Akkermansia*, Muribaculaceae, and Lachnospiraceae families play an important role in modulating inflammatory responses and regulating gut metabolites, including saturated and unsaturated fatty acids and cholesterol-related compounds. Furthermore, these results indicate that BCEVs may contribute to NASH improvement by influencing gut microbiota composition and correlated metabolites.

3.10. BCEVs mitigate immune response and increase intestinal integrity

Previous studies have suggested that *Akkermansia* promotes intestinal mucin production and strengthens intestinal tight junctions (Segers and de Vos, 2023). To determine whether the reduction in bacterial and inflammatory responses in the liver was attributed to BCEV administration to the intestine, the expression of genes encoding pro-inflammatory cytokines and tight junction proteins in the intestine was quantified. The analysis showed that the expression of *Tnfa*, the gene encoding a pro-inflammatory cytokine, tended to increase (Fig. 11a) in the NASH group, although not significantly. Similarly, *Il6* expression was elevated in the NASH group (Fig. 11b). In contrast, BCEV treatment significantly decreased the expression of both *Tnfa* and *Il6*. Additionally, the expression of *Muc2*, *Cldn1*, and *Ocln*, genes encoding tight junction proteins, showed no significant differences between the NASH and CON groups, but their expression was significantly increased following BCEV treatment (Fig. 11c–e). These results suggest that BCEVs alleviate intestinal inflammation and enhance intestinal integrity, likely due to the increased abundance of *Akkermansia* in the gut microbiota.

4. Discussion

In this study, a multi-omics approach was employed to investigate whether BCEVs, known to influence gut microbiota, could alleviate gut microbiota imbalance associated with NASH and improve its symptoms. Oral administration of BCEVs for 3 wks, combined with a NASH-inducing diet, significantly reduced liver weight and hepatic lipid content, while improving NAS scores, including components such as steatosis, inflammation, and fibrosis. Additionally, BCEV treatment ameliorated hepatotoxicity and inflammatory responses. Transcriptomics analysis revealed that BCEVs downregulated genes related to lipid metabolism, bacterial response, and inflammation in the intestine. In the liver, BCEVs attenuated NASH-induced inflammation and fibrosis. Metagenomic and metabolomic analyses showed that BCEV treatment significantly increased the abundance of *Akkermansia* in the intestine while decreasing metabolites related to intestinal lipid metabolism and enhancing cholesterol excretion. BCEVs also promoted the production of intestinal tight junction proteins and mucin. Overall, BCEV treatment enhanced intestinal barrier function, alleviating NASH-induced intestinal inflammation and inhibiting liver inflammation and fibrosis by reducing the transport of endotoxins to the liver.

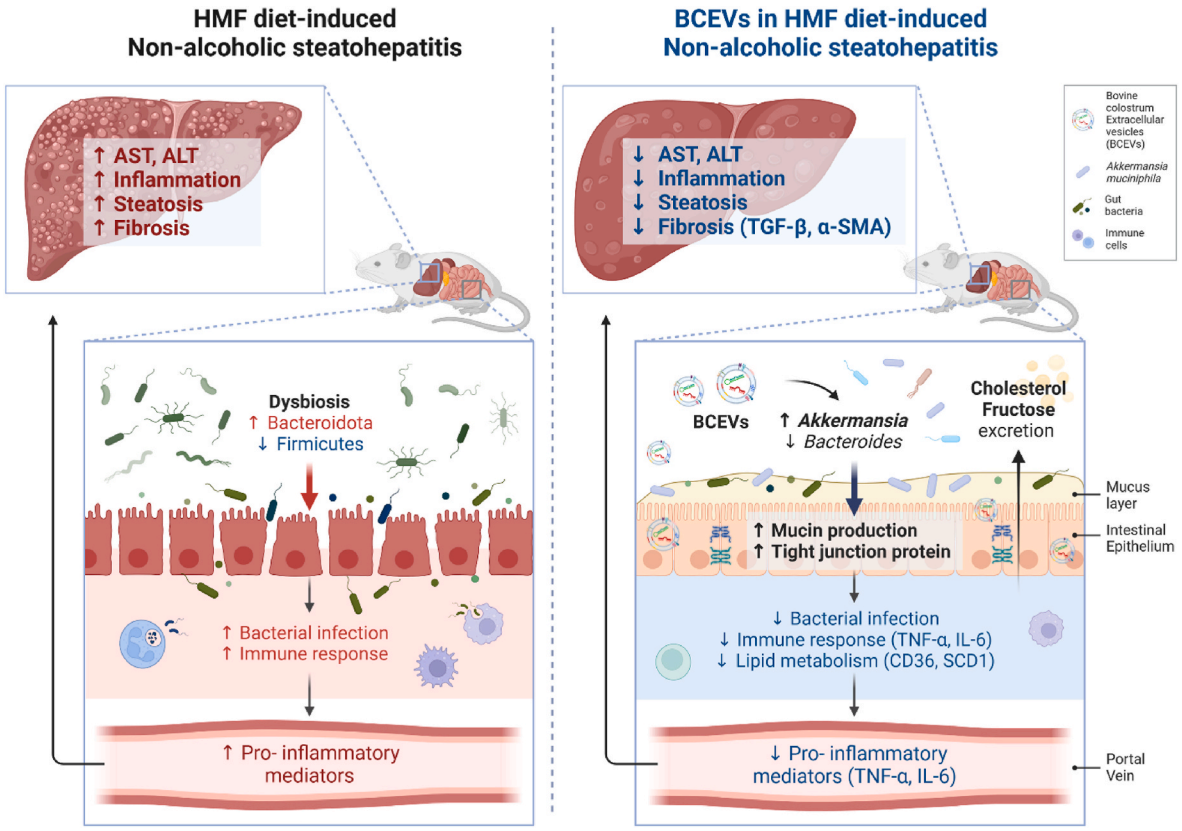

Fig. 12. Schematic diagram of the outcomes of an integrated multi-omics analysis investigating the role of bovine colostrum extracellular vesicles in a high-fat-fructose diet-induced model of non-alcoholic steatohepatitis.
The analysis reveals that bovine colostrum EVs attenuate both systemic immune responses and hepatic inflammatory responses through modulation of gut microbiota, particularly *Akkermansia* spp., and improvement of gut barrier function. Consequently, these effects contribute to the suppression of liver steatosis and fibrosis.

NAFLD and NASH are chronic liver diseases with a rapidly increasing global prevalence (Takahashi and Fukusato, 2014). While the exact pathogenesis remains unclear, known contributing factors include lipotoxicity, insulin resistance, genetic predisposition, impaired fat metabolism, dietary influences, and disturbance in the gut–liver axis due to gut microbiota imbalance (Takaki et al., 2014). Gut dysbiosis is specifically known to increase intestinal permeability, allowing endotoxins (e.g., LPS) to enter the liver via the portal vein, triggering inflammation and cellular damage (Jones and Neish, 2021). The overgrowth of Gram-negative bacteria exacerbates this process by increasing the production of hepatotoxins, such as LPS, which activate TLR-4 and initiate the production of pro-inflammatory cytokines (Duarte et al., 2019). Chronic inflammation leads to excessive extracellular matrix deposition, resulting in liver fibrosis and cirrhosis (Tanwar et al., 2020).

Several studies have demonstrated that milk-derived EVs can alleviate dysbiosis and reduce inflammatory responses in the gut. In mice, milk EVs increased the abundance of beneficial microorganisms, such as *Akkermansia*, *Muribaculum*, and *Turicibacter*, while decreasing the abundance of harmful microorganisms, such as *Desulfovibrio* (Du et al., 2021). EVs also alleviated colitis by promoting the growth of *Dubosiella*, *Bifidobacterium*, and *Lachnoclostridium* in the gut of a mouse model of colitis (Du et al., 2022). Furthermore, milk EV treatment enhanced gut integrity and helped prevent bacterial infections by modulating tight junctions (Hao et al., 2024). In ovariectomized mice, milk EV treatment reduced intestinal permeability by modulating tight junction proteins, leading to reduced endotoxin levels in serum and feces. Additionally, EV treatment promotes the recovery of beneficial bacteria, such as Bacteroidetes and *Alloprevotella*, in the gut microbiota (Hao et al., 2024). Consistent with these findings, this study showed that BCEVs alleviated the NASH-induced gut dysbiosis and improved the intestinal inflammatory response.

Fecal metabolome analysis revealed increased levels of cholesterol and fatty acids, such as 11-eicosenoic acid, in the BCEV treatment group. These changes are likely linked to the reduced expression of genes related to intestinal lipid and cholesterol metabolism. Intestinal transcriptome analysis following EV treatment revealed reduced expression of the *SCD1* and *CD36* genes, which are associated with fatty acid biosynthesis and transport, respectively. Additionally, genes related to lipoprotein lipase (*LPL*), which converts triacylglycerol to fatty acids in cholesterol metabolism, were downregulated (data not shown). A previous study reported that *Akkermansia muciniphila* increases lipid excretion by modulating *CD36* expression and reducing intestinal lipid absorption (Watanabe et al., 2023). However, in the present study, no significant changes were observed in triglyceride or total cholesterol levels in the liver or serum following EV treatment. These results indicate that while EVs and their associated gut microbiota alternations influenced lipid and cholesterol metabolism and related gene expression in the gut, they did not significantly affect lipid and cholesterol metabolism in the liver or blood (Figs. 2 and 3). Given the relatively short experimental duration, further confirmation of the effects of EVs on lipid and cholesterol metabolism through extended studies focusing on lipid metabolism in the liver and blood is warranted.

The gut microbiota composition in NASH patients differs from that of healthy individuals, particularly in the Firmicutes-to-Bacteroidetes ratio (Zhu et al., 2013). Notably, an increased abundance of *Bacteroides* has been observed in NASH patients (Boursier et al., 2016; Kang et al., 2023). In the NASH group, the significantly enriched *Bilophila* and *Erysipelatoclostridium* are known to be associated with high-fat diet consumption and intestinal inflammation (Caesar et al., 2015; Zhu et al., 2023). Furthermore, the reduction of beneficial bacteria such as

Alistipes, *Bifidobacterium*, *Muribaculum*, and *Ruminococcus*, which are depleted in the NASH group, has been reported to contribute to increased intestinal inflammation and metabolic dysregulation (Lin et al., 2025; Volk et al., 2019; Xu et al., 2024). Interestingly, our findings indicate that *Bacteroides*, which was excessively enriched following NASH induction, was markedly reduced after BCEV treatment. In addition, BCEVs administration decreased the overgrowth of *Parabacteroides*, which are associated with NASH (Li et al., 2024; Wong et al., 2013), as well as the potential harmful bacterium *Erysipelatoclostridium*, which has been implicated in gut dysbiosis and inflammation (Chen et al., 2024; Kang et al., 2021; Zhu et al., 2023). These findings suggest that BCEVs play a role in modulating gut microbiota composition, potentially contributing to gut homeostasis and mitigating NASH-associated dysbiosis.

Previous studies have linked EV treatment to an increased abundance of *Akkermansia* in the gut microbiota. Our group previously demonstrated that administering BCEVs to mice with DSS-induced colitis significantly increased the abundance of *Akkermansia*. Similarly, feeding mature milk-derived EVs to mice and inducing colitis also elevated intestinal *Akkermansia* levels (Liu et al., 2023; Tong et al., 2021). Consistent with these findings, BCEV treatment in the present study increased the abundance of *Akkermansia* in the gut microbiota. *Akkermansia muciniphila* is known to remodel the intestinal mucosa by promoting mucin degradation and mucin regeneration through stimulation of intestinal goblet cells (Segers and de Vos, 2023). In a previous study, oral administration of *A. muciniphila* to non-obese diabetic mice increased the expression of Reg3γ, a peptide that regulates intestinal epithelial function, while promoting mucin production and reducing serum endotoxin levels (Hanninen et al., 2018). Similarly, in a mouse model of high-fat diet-induced NASH, *A. muciniphila* administration upregulated the mRNA expression of intestinal tight junction proteins and decreased serum LPS concentrations (Qu et al., 2023). In addition to these findings, *A. muciniphila* has been shown to directly regulate intestinal barrier function by upregulating the expression of *MUC2*, *BIRC3*, and *TNFAIP3*, key genes involved in mucosal integrity (Martin-Gallausiaux et al., 2022). In the present study, transcriptome analysis of the colon revealed that bacterial responses, which were significantly elevated in NASH-induced mice, were markedly reduced following oral administration of high concentrations of EVs. Moreover, the intestinal expression of *Cldn1*, *Ocln*, and *Muc2*, genes encoding tight junction proteins, was significantly higher in EVH group compared to NASH-induced mice. These findings suggest that EVs inhibit the translocation of endotoxins from the gut into the bloodstream and liver. However, further studies, including direct evaluation of endotoxin levels in the blood and liver, are necessary to confirm this mechanism.

This study has certain limitations that should be considered. First, this study employed a diet-induced NASH model to investigate the effects of orally administered BCEV on the gut microbiome and NASH progression. Further studies using additional NASH models, such as the gene knockout mouse model, are required to validate the universality of the study results. Second, to identify the direct mechanistic association between changes in the gut microbiome and improved intestinal barrier function due to BECVs, further investigations using fecal microbiota transplantation or germ-free mouse models will be required. Finally, this study provides evidence supporting the therapeutic potential of BCEVs in NASH, but further studies on large-scale production, safety assessment, and clinical feasibility are essential for their translational application.

5. Conclusion

In conclusion, high doses of BCEVs exerted protective effects, inhibiting the development and progression of NASH through several mechanisms. BCEVs regulated the gut microbiome, particularly by increasing the abundance of *Akkermansia*, a bacterium associated with improved gut health. BCEV treatment also reduced intestinal inflammation and increased the production of tight junction proteins and mucins, thereby strengthening the intestinal barrier. These changes significantly reduced liver inflammation and fibrosis, while also improving lipid metabolism and liver health. Additionally, BCEVs promoted cholesterol excretion and alleviated disruptions in intestinal lipid metabolism, contributing to overall metabolic homeostasis (Fig. 12). These findings support the potential of BCEVs as a functional substance for alleviating NASH and suggest that BCEVs may serve as a novel therapeutic intervention to its mitigation.

CRediT authorship contribution statement

Daye Mun: Writing – original draft, Methodology, Investigation, Formal analysis, Conceptualization. **Sangdon Ryu:** Writing – original draft, Methodology, Investigation, Formal analysis, Conceptualization. **Daniel Junpyo Lee:** Writing – review & editing, Visualization, Software, Methodology, Data curation. **Min-Jin Kwak:** Writing – review & editing, Visualization, Software, Methodology. **Hyejin Choi:** Writing – review & editing, Visualization, Software, Methodology. **An Na Kang:** Writing – review & editing, Visualization, Software, Methodology. **Dong-Hyun Lim:** Visualization, Software, Methodology. **Sangnam Oh:** Writing – review & editing, Supervision, Project administration, Investigation, Conceptualization. **Younghoon Kim:** Writing – review & editing, Supervision, Project administration, Investigation, Funding acquisition, Conceptualization.

Ethical approval and consent to participate

All protocols for animal experiments were thoroughly evaluated and approved by the Institutional Animal Care and Use Committee of Seoul National University (SNU-221101-2-2).

Consent for publication

Not applicable.

Funding

This research was supported by a National Research Foundation of Korea Grant, funded by the Korean government (MEST) (NRF-2021R1A2C3011051) and Basic Science Research Program through the National Research Foundation of Korea (NRF) funded by the Ministry of Education (2022M3A9I5018286).

Declaration of competing interest

The authors declare that they have no known competing financial interests or personal relationships that could have appeared to influence the work reported in this paper.

Acknowledgments

None.

Data availability

Data will be made available on request.

References

Bolger, A.M., Lohse, M., Usadel, B., 2014. Trimmomatic: a flexible trimmer for Illumina sequence data. Bioinformatics 30, 2114–2120.

Boursier, J., Mueller, O., Barret, M., Machado, M., Fizanne, L., Araujo-Perez, F., Guy, C. D., Seed, P.C., Rawls, J.F., David, L.A., Hunault, G., Oberti, F., Cales, P., Diehl, A.M., 2016. The severity of nonalcoholic fatty liver disease is associated with gut dysbiosis and shift in the metabolic function of the gut microbiota. Hepatology 63, 764–775.

Brown, G.T., Kleiner, D.E., 2016. Histopathology of nonalcoholic fatty liver disease and nonalcoholic steatohepatitis. Metabolism 65, 1080–1086.
Brunt, E.M., Kleiner, D.E., Wilson, L.A., Belt, P., Neuschwander-Tetri, B.A., Network, N.C. R., 2011. Nonalcoholic fatty liver disease (NAFLD) activity score and the histopathologic diagnosis in NAFLD: distinct clinicopathologic meanings. Hepatology 53, 810–820.
Bugianesi, E., Leone, N., Vanni, E., Marchesini, G., Brunello, F., Carucci, P., Musso, A., De Paolis, P., Capussotti, L., Salizzoni, M., Rizzetto, M., 2002. Expanding the natural history of nonalcoholic steatohepatitis: from cryptogenic cirrhosis to hepatocellular carcinoma. Gastroenterology 123, 134–140.
Caesar, R., Tremaroli, V., Kovatcheva-Datchary, P., Cani, P.D., Bäckhed, F., 2015. Crosstalk between gut microbiota and dietary lipids aggravates WAT inflammation through TLR signaling. Cell Metab. 22, 658–668.
Chen, D., Wang, Y., Yang, J., Ou, W., Lin, G., Zeng, Z., Lu, X., Chen, Z., Zou, L., Tian, Y., 2024. Shenling Baizhu San ameliorates non-alcoholic fatty liver disease in mice by modulating gut microbiota and metabolites. Front. Pharmacol. 15, 1343755.
Du, C., Quan, S., Nan, X., Zhao, Y., Shi, F., Luo, Q., Xiong, B., 2021. Effects of oral milk extracellular vesicles on the gut microbiome and serum metabolome in mice. Food Funct. 12, 10938–10949.
Du, C., Wang, K., Zhao, Y., Nan, X., Chen, R., Quan, S., Xiong, B., 2022. Supplementation with milk-derived extracellular vesicles shapes the gut microbiota and regulates the transcriptomic landscape in experimental colitis. Nutrients 14.
Duarte, S.M.B., Stefano, J.T., Oliveira, C.P., 2019. Microbiota and nonalcoholic fatty liver disease/nonalcoholic steatohepatitis (NAFLD/NASH). Ann. Hepatol. 18, 416–421.
Gandham, S., Su, X., Wood, J., Nocera, A.L., Alli, S.C., Milane, L., Zimmerman, A., Amiji, M., Ivanov, A.R., 2020. Technologies and standardization in research on extracellular vesicles. Trends Biotechnol. 38, 1066–1098.
Han, H., Jiang, Y., Wang, M., Melaku, M., Liu, L., Zhao, Y., Everaert, N., Yi, B., Zhang, H., 2023. Intestinal dysbiosis in nonalcoholic fatty liver disease (NAFLD): focusing on the gut-liver axis. Crit. Rev. Food Sci. Nutr. 63, 1689–1706.
Hanninen, A., Toivonen, R., Poysti, S., Belzer, C., Plovier, H., Ouwerkerk, J.P., Emani, R., Cani, P.D., De Vos, W.M., 2018. Akkermansia muciniphila induces gut microbiota remodelling and controls islet autoimmunity in NOD mice. Gut 67, 1445–1453.
Hao, H., Liu, Q., Zheng, T., Li, J., Zhang, T., Yao, Y., Liu, Y., Lin, K., Liu, T., Gong, P., Zhang, Z., Yi, H., 2024. Oral milk-derived extracellular vesicles inhibit osteoclastogenesis and ameliorate bone loss in ovariectomized mice by improving gut microbiota. J. Agric. Food Chem. 72, 4726–4736.
Iverson, S.J., Lang, S.L., Cooper, M.H., 2001. Comparison of the Bligh and Dyer and Folch methods for total lipid determination in a broad range of marine tissue. Lipids 36, 1283–1287.
Jiang, X., Wu, Y., Zhong, H., Zhang, X., Sun, X., Liu, L., Cui, X., Chi, X., Ji, C., 2023. Human milk-derived extracellular vesicles alleviate high fat diet-induced non-alcoholic fatty liver disease in mice. Mol. Biol. Rep. 50, 2257–2268.
Jones, R.M., Neish, A.S., 2021. Gut microbiota in intestinal and liver disease. Annu. Rev. Pathol. 16, 251–275.
Jr, G.D., Sherman, B.T., Hosack, D.A., Yang, J., Gao, W., Lane, H.C., Lempicki, R.A., 2003. DAVID: database for annotation, visualization, and integrated discovery. Genome Biol. 4, R60.
Kang, G.G., Trevaskis, N.L., Murphy, A.J., Febbraio, M.A., 2023. Diet-induced gut dysbiosis and inflammation: key drivers of obesity-driven NASH. iScience 26.
Kang, K., Sun, Y., Pan, D., Sang, L.-X., Sun, M.-J., Li, Y.-L., Chang, B., 2021. Distinctive gut microbial dysbiosis between chronic alcoholic fatty liver disease and metabolic-associated fatty liver disease in mice. Exp. Ther. Med. 21, 418.
Kim, D., Langmead, B., Salzberg, S.L., 2015. HISAT: a fast spliced aligner with low memory requirements. Nat. Methods 12, 357–360.
Li, H., Wang, M., Chen, P., Zhu, M., Chen, L., 2024. A high-dose of ursodeoxycholic acid treatment alleviates liver inflammation by remodeling gut microbiota and bile acid profile in a mouse model of non-alcoholic steatohepatitis. Biomed. Pharmacother. 174, 116617.
Lin, X., Xu, M., Lan, R., Hu, D., Zhang, S., Zhang, S., Lu, Y., Sun, H., Yang, J., Liu, L., 2025. Gut commensal Alistipes shahii improves experimental colitis in mice with reduced intestinal epithelial damage and cytokine secretion. mSystems, e01607, 01624.
Liu, J., Wu, A., Cai, J., She, Z.G., Li, H., 2022. The contribution of the gut-liver axis to the immune signaling pathway of NAFLD. Front. Immunol. 13, 968799.
Liu, Q., Hao, H., Li, J., Zheng, T., Yao, Y., Tian, X., Zhang, Z., Yi, H., 2023. Oral administration of bovine milk-derived extracellular vesicles attenuates cartilage degeneration via modulating gut microbiota in DMM-induced mice. Nutrients 15.
Martin-Gallausiaux, C., Garcia-Weber, D., Lashermes, A., Larraufie, P., Marinelli, L., Teixeira, V., Rolland, A., Béguet-Crespel, F., Brochard, V., Quatremare, T., 2022. Akkermansia muciniphila upregulates genes involved in maintaining the intestinal barrier function via ADP-heptose-dependent activation of the ALPK1/TIFA pathway. Gut Microbes 14, 2110639.
Mun, D., Kang, M., Shin, M., Choi, H.J., Kang, A.N., Ryu, S., Unno, T., Maburutse, B.E., Oh, S., Kim, Y., 2023. Alleviation of DSS-induced colitis via bovine colostrum-derived extracellular vesicles with microRNA let-7a-5p is mediated by regulating Akkermansia and β-hydroxybutyrate in gut environments. Microbiol. Spectr. 11, e00121, 00123.
Pang, Z., Chong, J., Zhou, G., de Lima Morais, D.A., Chang, L., Barrette, M., Gauthier, C., Jacques, P.-É., Li, S., Xia, J., 2021. MetaboAnalyst 5.0: narrowing the gap between raw spectra and functional insights. Nucleic Acids Res. 49, W388–W396.
Parks, D.H., Tyson, G.W., Hugenholtz, P., Beiko, R.G., 2014. STAMP: statistical analysis of taxonomic and functional profiles. Bioinformatics 30, 3123–3124.
Pertea, M., Pertea, G.M., Antonescu, C.M., Chang, T.-C., Mendell, J.T., Salzberg, S.L., 2015. StringTie enables improved reconstruction of a transcriptome from RNA-seq reads. Nat. Biotechnol. 33, 290–295.
Poeta, M., Pierri, L., Vajro, P., 2017. Gut-liver Axis derangement in non-alcoholic fatty liver disease. Children (Basel) 4.
Qu, D., Chen, M., Zhu, H., Liu, X., Cui, Y., Zhou, W., Zhang, M., 2023. Akkermansia muciniphila and its outer membrane protein Amuc_1100 prevent high-fat diet-induced nonalcoholic fatty liver disease in mice. Biochem. Biophys. Res. Commun. 684, 149131.
Quast, C., Pruesse, E., Yilmaz, P., Gerken, J., Schweer, T., Yarza, P., Peplies, J., Glöckner, F.O., 2012. The SILVA ribosomal RNA gene database project: improved data processing and web-based tools. Nucleic Acids Res. 41, D590–D596.
Robinson, M.D., McCarthy, D.J., Smyth, G.K., 2010. edgeR: a Bioconductor package for differential expression analysis of digital gene expression data. Bioinformatics 26, 139–140.
Segers, A., de Vos, W.M., 2023. Mode of action of Akkermansia muciniphila in the intestinal dialogue: role of extracellular proteins, metabolites and cell envelope components. Microbiome Res. Rep. 2, 6.
Sheka, A.C., Adeyi, O., Thompson, J., Hameed, B., Crawford, P.A., Ikramuddin, S., 2020. Nonalcoholic steatohepatitis: a review. JAMA 323, 1175–1183.
Song, Q., Zhang, X., 2022. The role of gut-liver Axis in gut microbiome dysbiosis associated NAFLD and NAFLD-HCC. Biomedicines 10.
Takahashi, Y., Fukusato, T., 2014. Histopathology of nonalcoholic fatty liver disease/nonalcoholic steatohepatitis. World J. Gastroenterol. 20, 15539–15548.
Takaki, A., Kawai, D., Yamamoto, K., 2014. Molecular mechanisms and new treatment strategies for non-alcoholic steatohepatitis (NASH). Int. J. Mol. Sci. 15, 7352–7379.
Tanwar, S., Rhodes, F., Srivastava, A., Trembling, P.M., Rosenberg, W.M., 2020. Inflammation and fibrosis in chronic liver diseases including non-alcoholic fatty liver disease and hepatitis C. World J. Gastroenterol. 26, 109.
Thapa, B., 2005. Health factors in colostrum. Indian J. Pediatr. 72, 579–581.
Tong, L., Hao, H., Zhang, Z., Lv, Y., Liang, X., Liu, Q., Liu, T., Gong, P., Zhang, L., Cao, F., Pastorin, G., Lee, C.N., Chen, X., Wang, J.W., Yi, H., 2021. Milk-derived extracellular vesicles alleviate ulcerative colitis by regulating the gut immunity and reshaping the gut microbiota. Theranostics 11, 8570–8586.
Tong, L., Zhang, S., Liu, Q., Huang, C., Hao, H., Tan, M.S., Yu, X., Lou, C.K.L., Huang, R., Zhang, Z., 2023. Milk-derived extracellular vesicles protect intestinal barrier integrity in the gut-liver axis. Sci. Adv. 9, eade5041.
Volk, J.K., Nyström, E.E., van der Post, S., Abad, B.M., Schroeder, B.O., Johansson, Å., Svensson, F., Jäverfelt, S., Johansson, M.E., Hansson, G.C., 2019. The Nlrp6 inflammasome is not required for baseline colonic inner mucus layer formation or function. J. Exp. Med. 216, 2602–2618.
Wang, L., Shi, Z., Wang, X., Mu, S., Xu, X., Shen, L., Li, P., 2021. Protective effects of bovine milk exosomes against oxidative stress in IEC-6 cells. Eur. J. Nutr. 60, 317–327.
Watanabe, Y., Fujisaka, S., Morinaga, Y., Watanabe, S., Nawaz, A., Hatta, H., Kado, T., Nishimura, A., Bilal, M., Aslam, M.R., 2023. Isoxanthohumol improves obesity and glucose metabolism via inhibiting intestinal lipid absorption with a bloom of Akkermansia muciniphila in mice. Mol. Metabol. 77, 101797.
Wiklander, O.P., Brennan, M.Á., Lötvall, J., Breakefield, X.O., El Andaloussi, S., 2019. Advances in therapeutic applications of extracellular vesicles. Sci. Transl. Med. 11, eaav8521.
Wong, V.W.-S., Tse, C.-H., Lam, T.T.-Y., Wong, G.L.-H., Chim, A.M.-L., Chu, W.C.-W., Yeung, D.K.-W., Law, P.T.-W., Kwan, H.-S., Yu, J., 2013. Molecular characterization of the fecal microbiota in patients with nonalcoholic steatohepatitis–a longitudinal study. PLoS One 8, e62885.
Xu, X., Wang, Y., Wu, X., Cai, T., Dong, L., Liang, S., Zhu, L., Song, X., Dong, Y., Zheng, Y., 2024. Administration of Alistipes indistinctus prevented the progression from nonalcoholic fatty liver disease to nonalcoholic steatohepatitis by enhancing the gut barrier and increasing Lactobacillus spp. Biochem. Biophys. Res. Commun. 741, 151033.
Yoo, J., Lee, J., Zhang, M., Mun, D., Kang, M., Yun, B., Kim, Y.-A., Kim, S., Oh, S., 2022. Enhanced γ-aminobutyric acid and sialic acid in fermented deer antler velvet and immune promoting effects. J. Anim. Sci. Technol. 64, 166.
Zhu, L., Baker, S.S., Gill, C., Liu, W., Alkhouri, R., Baker, R.D., Gill, S.R., 2013. Characterization of gut microbiomes in nonalcoholic steatohepatitis (NASH) patients: a connection between endogenous alcohol and NASH. Hepatology 57, 601–609.
Zhu, X., Cai, J., Wang, Y., Liu, X., Chen, X., Wang, H., Wu, Z., Bao, W., Fan, H., Wu, S., 2023. A high-fat diet increases the characteristics of gut microbial composition and the intestinal damage associated with non-alcoholic fatty liver disease. Int. J. Mol. Sci. 24, 16733.